

From the middle stratosphere to the surface, using nitrous oxide to constrain the stratosphere-troposphere exchange of ozone

Daniel J. Ruiz¹ and Michael J. Prather¹

¹Department of Earth System Science, University of California, Irvine, CA 92697-3100, USA

Correspondence to: Daniel J. Ruiz (djruiz@uci.edu)

Abstract

Stratosphere-troposphere exchange (STE) is an important source of tropospheric ozone, affecting all of atmospheric chemistry, climate, and air quality. The study of impacts needs STE fluxes to be resolved by latitude and month, and for this we rely on global chemistry models, whose results diverge greatly. Overall, we lack guidance from model-measurement metrics that inform us about processes and patterns related to the STE flux of ozone (O₃). In this work, we use modeled tracers (N₂O, CFCl₃) whose distributions and budgets can be constrained by satellite and surface observations, allowing us to follow stratospheric signals across the tropopause. The satellite derived photochemical loss of N₂O on annual and quasi-biennial cycles can be matched by the models. The STE flux of N₂O-depleted air in our chemistry transport model drives surface variability that closely matches observed fluctuations on both annual and quasi-biennial cycles, confirming the modeled flux. The observed tracer correlations between N₂O and O₃ in the lowermost stratosphere provide a hemispheric scaling of the N₂O STE flux to that of O₃. For N₂O and CFCl₃, we model greater southern hemispheric STE fluxes, a result supported by some metrics, but counter to prevailing theory of wave-driven stratospheric circulation. The STE flux of O₃, however, is predominantly northern hemispheric, but evidence shows that this is caused by the Antarctic ozone hole reducing southern hemispheric O₃ STE by 14%. Our best estimate of the current STE O₃ flux based on a range of constraints is 400 Tg(O₃)/yr with a one-sigma uncertainty of ±15% and with a NH:SH ratio ranging from 50:50 to 60:40. We identify a range of observational metrics that can better constrain the modeled STE O₃ flux in future assessments.

1. Introduction & Background

The influx of stratospheric ozone (O₃) into the troposphere affects its distribution, variability, lifetime, and thus its role in driving climate change and surface air pollution (Zeng et al., 2010; Hess et al., 2015; Williams et al., 2019). The net stratosphere-to-troposphere exchange (STE) flux of O₃ has a regular seasonal cycle in each hemisphere that is an important part of the tropospheric O₃ budget (Stohl et al., 2003). Such fluxes are not directly observable, and we rely on observational estimates using trace-gas ratios, in particular the O₃:N₂O ratio in the lower stratosphere (Murphy and Fahey, 1994; McLinden et al., 2000), or dynamical calculations using measured/modeled winds and O₃ abundances (Gettelman et al., 1997; Olsen et al., 2004; Yang et al., 2016). The uncertainty in these estimates does not effectively constrain the wide range found in the models being used to project future ozone (Young et al., 2013, 2018; Griffiths et al., 2021). Here we present the case for using the observed variations in nitrous oxide (N₂O) from the middle stratosphere to the surface in order to constrain the STE flux of O₃. A similar case

has been made for the radionuclide ^7Be (Liu et al., 2016), but N_2O has a wealth of model-observation metrics on hemispheric, seasonal, and interannual scales that constrains its STE flux very well (Prather et al., 2015; Ruiz et al., 2021).

Ozone-rich stratospheric air has been photochemically aged and is depleted in trace gases such as N_2O and chlorofluorocarbons (CFCs). For these trace gases, the overall circulation from tropospheric sources to stratospheric destruction and back is part of the lifecycle that maintains their global abundance (Holton, 1990). For N_2O and CFCs, this cycle of (i) loss in the middle to upper stratosphere, (ii) transport to the lowermost stratosphere (Holton et al., 1995), and then (iii) influx into the troposphere produces surface variations not related to surface emissions (Hamilton and Fan, 2000; Nevison et al., 2004; Hirsch et al., 2006; Montzka et al., 2018; Ray et al., 2020; Ruiz et al., 2021). In this work we relate our modeled STE fluxes to variations at the surface and throughout the stratosphere, linking the fluxes of N_2O to O_3 through stratospheric measurements. Our goal is to develop a set of model metrics founded on observations that are related to the STE O_3 flux and can be used with an ensemble of models to determine a better, constrained estimate for the flux, including seasonal, interannual, and hemispheric patterns. This approach is similar to efforts involving the ozone depletion recovery time (Strahan et al., 2011) and projections of future warming (Liang et al., 2020; Tokarska et al., 2020).

In a previous work (Ruiz et al., 2021, hence R2021) we showed that historical simulations with three chemistry transport models (CTMs) were able to match the interannual surface variations observed in N_2O . These were clearly driven by the stratospheric quasi-biennial oscillation (QBO) which appears to be the major interannual signal in stratospheric circulation and STE (Kinnerson and Tung, 1999; Baldwin et al., 2001; Olsen et al., 2019). In this work, we calculate the monthly latitudinal STE fluxes of O_3 , N_2O , and CFCl_3 (F11), establish a coherent picture relating fluxes to observed abundances, and summarize the methods in Section 2. In section 3, we examine the annual and interannual cycles as well as geographic patterns of modeled STE flux. In section 4, we relate the surface variability of N_2O to its STE flux. We find some evidence to support our model result that the STE flux of depleted- N_2O air is greater in the southern hemisphere than in the northern, thus altering the asymmetry in surface emissions in the source inversions (Nevison et al., 2007; Thompson et al., 2014). In section 5, we examine the lowermost stratosphere to understand the large north-south asymmetry found in O_3 STE versus N_2O or F11 STE, and find a clear signal of the Antarctic ozone hole in STE. In section 6, we examine the consistency of the model calculations of STE flux and derive a best estimate for the O_3 flux from this and previous studies. We summarize a sequence of model metrics, primarily using O_3 and N_2O , that can narrow the range in the tropospheric O_3 budget terms for the multi-model intercomparison projects used in tropospheric chemistry and climate assessments.

2. Methods

The modeled STE fluxes here are calculated with the UCI (University of California Irvine) CTM driven by 3-hour forecast fields from the European Centre for Medium-range Weather Forecasts (ECMWF) Integrated Forecast System (IFS Cycle 38r1 T159L60) for years 1990-2017, as are the calculations in R2021. The CTM uses the IFS native 160x320 Gauss grid ($\sim 1.1^\circ$) with 60 layers, about 35 of which are in the troposphere. The stratospheric chemistry uses the linearized model Linoz v3 and includes O_3 , N_2O , NO_y , CH_4 , and F11 as transported trace gases (Hsu and

Prather, 2010; Prather et al., 2015; Ruiz et al., 2021). There is no tropospheric chemistry, but rather a boundary-layer e-fold to a specified abundance, or a surface boundary reset to an abundance. Equivalent effective stratospheric chlorine levels are high enough to drive an Antarctic ozone hole, which is observed throughout this period. Thus, the ozone-hole chemistry in Linoz v3 is activated for all years, and the amount of O₃ depleted depends on the Antarctic meteorology of that year (Hsu and Prather, 2010).

The STE flux is calculated using the e90 definition of tropospheric grid cells (Prather et al., 2011) and the change in tropospheric tracer mass from before to after each tracer transport step as developed at UCI (Hsu et al., 2005; Hsu and Prather, 2009; Hsu and Prather, 2014). This method is precise and geographically accurate for O₃ and is self-consistent with a CTM's tracer-transport calculation (Tang et al., 2013; Hsu and Prather, 2014). Extensive comparisons with other methods of calculating STE are shown in Hsu and Prather (2014). Annual-mean STE fluxes are calculated from the full 28-year (336 month) time series as 12-month running means, and the annual cycle of monthly fluxes is the average of the 28 values for each month.

R2021 modeled the surface signal of stratospheric loss with the decaying tracers, N₂OX and F11X (e.g., (Hamilton and Fan, 2000; Hirsch et al., 2006). These X-tracers have the identical stratospheric chemical loss frequencies as N₂O and CFC1₃, respectively, but no surface sources and are therefore affected only by the stratospheric sink and atmospheric transport. The multi-decade (F11X) to century (N₂OX) decays are easily rescaled using a 12-month smoothing filter to give stationary results and a tropospheric mean abundance of 320 ppb. We treat F11X like N₂OX with the same initial conditions and molecular weight. Budgets for N₂OX are reported, as in N₂O studies (Tian et al., 2020), as Tg of N as N₂O. These rescaled N₂OX and F11X tracers are designated simply as N₂O (not N₂O) and F11. Our F11 STE fluxes are thus unrealistically large compared to current CFC1₃ fluxes, but can be easily compared with our N₂O results.

When trying to calculate the STE flux of N₂O-depleted air across the tropopause, we found that the Hsu method was numerically noisy because the gradient across the tropopause, unlike that of O₃, was negligible. Thus, for this work we created the complementary tracers cN₂OX and cF11X: for each kg of the X-tracer (i.e., N₂OX) destroyed by photochemistry, 1 kg of its complementary tracer (cN₂OX) is created. Air parcels that are depleted in N₂OX (F11X) are therefore rich in cN₂OX (cF11X). After crossing the tropopause, cN₂OX and cF11X are removed through rapid uptake in the boundary layer, thus creating sharp gradients at the tropopause in parallel with that of O₃. As a check, we compared the boundary layer sinks of the c-tracers with their e90-derived STE fluxes and find that their sums are identical. The c-tracers and their STE fluxes are rescaled as are the X-tracers to give them a stationary time series corresponding to a tropospheric abundance of 320 ppb for their parallel X tracers. We designate these scaled tracers simply as cN₂O and cF11.

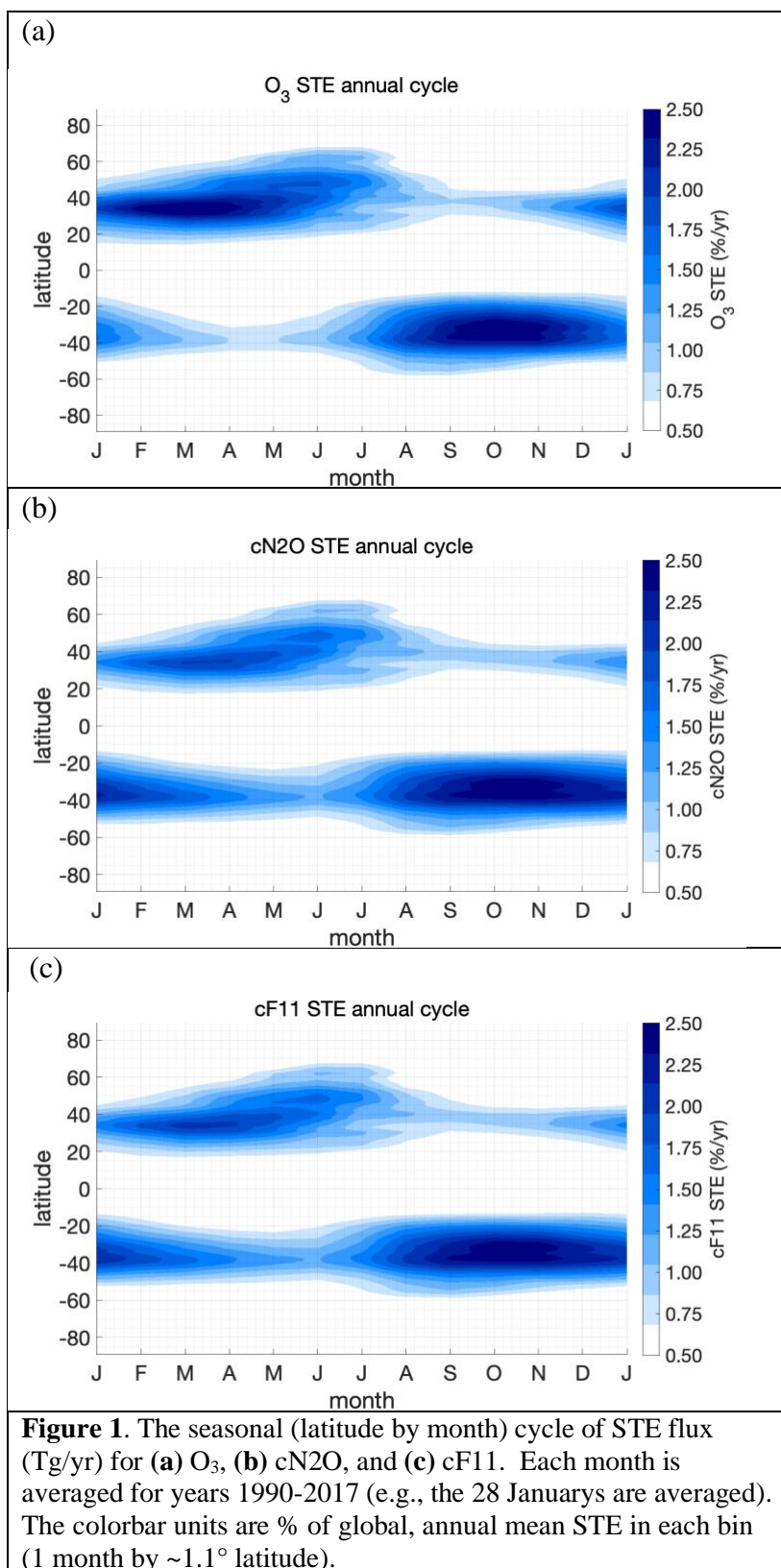
3. Modeled STE fluxes

3.1 Global and hemispheric means

The 28-year mean of global O₃ STE is 390±16 Tg/yr (positive flux means stratosphere to troposphere, the ± values are the standard deviation of the 28 annual means and do not represent

uncertainty). This value is well within the uncertainty in the observation-based estimates (Murphy and Fahey, 1994; Olsen et al., 2001), and far from the extreme ranges of the 34 models in the latest Tropospheric Ozone Assessment Report (Young et al., 2018), 150 to 940 Tg/yr. The global STE flux of cN₂O is 11.5 ± 0.7 Tg/yr, and that of cF11 is 23.5 ± 1.5 Tg/yr. These fluxes for cN₂O and cF11 match the total long-term troposphere-to-stratosphere flux of N₂O and F11 as derived from their stratospheric losses. The cF11 budget is about twice as large as cN₂O, because F11 is photolyzed rapidly in the lower-middle stratosphere (~24 km) instead of the upper stratosphere like N₂O (~32 km). The seasonal mean pattern of STE fluxes are shown in Figure 1. The large majority of STE flux enters the troposphere at 25°-45° latitude in each hemisphere, but there is a broadening of the northern flux to 65°N in Jun-Jul. The importance of this region about the sub-tropical jet for STE is supported by satellite data where stratospheric folding events (high O₃ in the upper troposphere) are found at the bends of the jet (Tang and Prather, 2010).

Given the small STE fluxes in the core tropics, the northern hemisphere (NH) and southern hemisphere (SH) fluxes are distinct. The annual mean of NH O₃ STE is 208 ± 11 Tg/yr and is slightly larger than the SH mean of 182 ± 11 Tg/yr. This NH:SH ratio of 53:47 is typically found in other studies (Gettelman et al., 1997; Hsu and Prather, 2009; Yang et al., 2016), although some have higher ratios like 58:42 (Hegglin and Shepherd, 2009; Meul et al., 2018). In contrast, for cN₂O and cF11, the NH flux (5.1 ± 0.4 Tg/yr and 10.6 ± 0.8 Tg/yr, respectively) is smaller than the SH flux (6.4 ± 0.5 Tg/yr and 12.9 ± 1.0 Tg/yr, respectively), giving a NH:SH ratio of about 45:55. The established view on STE is that the flux is wave-driven and under downward control, and thus the NH flux is much greater than the SH flux (see Table 1 of Holton et al., 1995; also Appenzeller et al., 1996). Our unexpected results require further analysis including evidence for hemispheric asymmetry in observations which is shown in section 4 along with other model metrics.



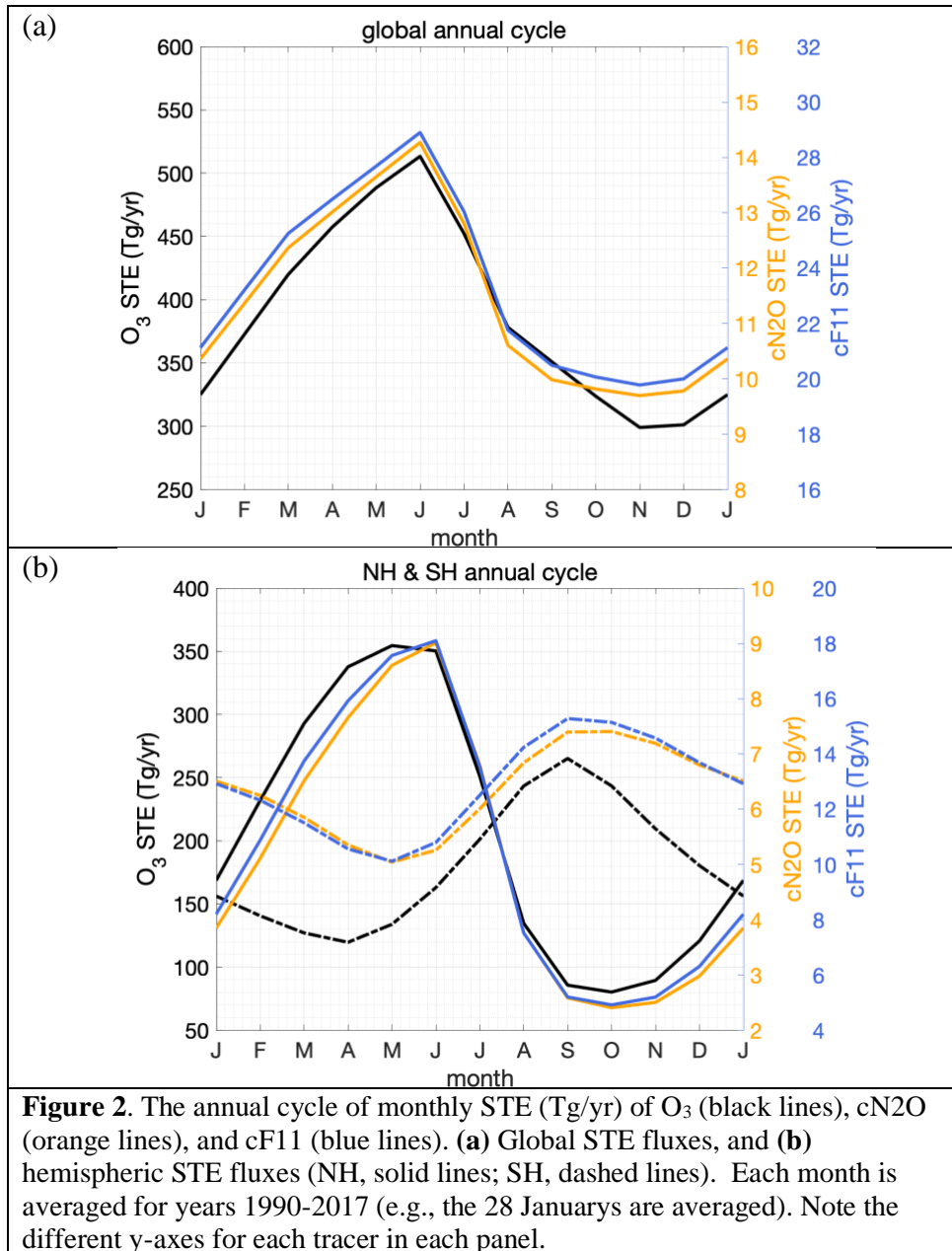
173
174

3.2 Seasonal cycle

The seasonal cycles of STE fluxes summed over global, NH, and SH are shown in Figure 2. The scales are given as the annual rate (as if the monthly rate were maintained for the year), and each species has a different axis. The right y-axes are kept at a N₂O:F11 ratio of 1:2. Despite large differences in the stratospheric chemistry across all three species, the seasonal cycle of STE is highly correlated (Pearson's correlation coefficient $cc > 0.98$, except for SH O₃), indicating that all three enter the troposphere from a seasonally near-uniform mixture of O₃:N₂O:F11 in the lowermost stratosphere.

Global STE peaks in June and reaches a minimum in November. The two hemispheres have dramatically different seasonal amplitudes and somewhat opposite phases. NH peak STE for all 3 species occurs in the late boreal spring (May-June), while that in the SH occurs at the start of austral spring (September-October). In the NH O₃ STE peaks a month before the c-tracers, and in the SH the whole annual cycle of O₃ is shifted a month earlier. The NH STE seasonal amplitude is very large for all species (~ 4:1 ratio max-to-min) with exchange almost ceasing in the fall. In contrast, the SH STE is more uniform year-round with a 1.5:1 ratio for cN₂O and cF11, and 2.2:1 for O₃. Other models with similar NH and SH O₃ fluxes show different seasonal amplitudes and phasing (see Fig. 6 of Tang et al., 2021), which will affect tropospheric O₃ abundances. It is important to develop observational metrics that test the seasonality of the lowermost stratosphere related to STE fluxes, and to establish monthly STE fluxes as a standard model diagnostic.

An interesting result here is the very tight correlation of the monthly cN₂O and cF11 STE while the O₃ STE is sometimes shifted. Loss of N₂O and F11 occurs at very different altitudes in the tropical stratosphere (~32 km and ~24 km, respectively), but both have similar seasonality in loss, driven mostly by the intensity of sunlight along the Earth's orbit (N₂O loss peaks in Feb and reaches a minimum in July, see Fig. 4 from Prather et al. (2015). Photochemical losses of N₂O and F11 drop quickly for air descending from the altitudes of peak loss in the tropics and hence the relative cN₂O and cF11 STE fluxes are locked in. O₃, however, continues to evolve photochemically from 24 km to 16 km (upper boundary of the lowermost stratosphere), through net photochemical production in the tropics and loss at mid- and high-latitudes that depends on sunlight and is thus seasonal. There may be observational evidence for the patterns modeled here in the correlation of these three tracers in the lower (16-20 km) and lowermost (12-16 km) extratropical stratosphere (see section 4).



3.3 Interannual variability

Interannual variability (IAV) of N_2O loss and its lifetime is associated primarily with the QBO (most recently, R2021). When the QBO is in its easterly (westerly) phase the entire overturning circulation is enhanced (suppressed) (Baldwin et al., 2001). This results in more (less) air rich in N_2O and F11 being transported from the troposphere to the lower or middle stratosphere, thereby increasing (decreasing) the N_2O and F11 sinks (Prather et al., 2015; Strahan et al., 2015). From the tropical stratosphere, the overturning circulation transports air depleted in N_2O and F11 into the lowermost extratropical stratosphere, where it enters the troposphere. R2021 showed that the

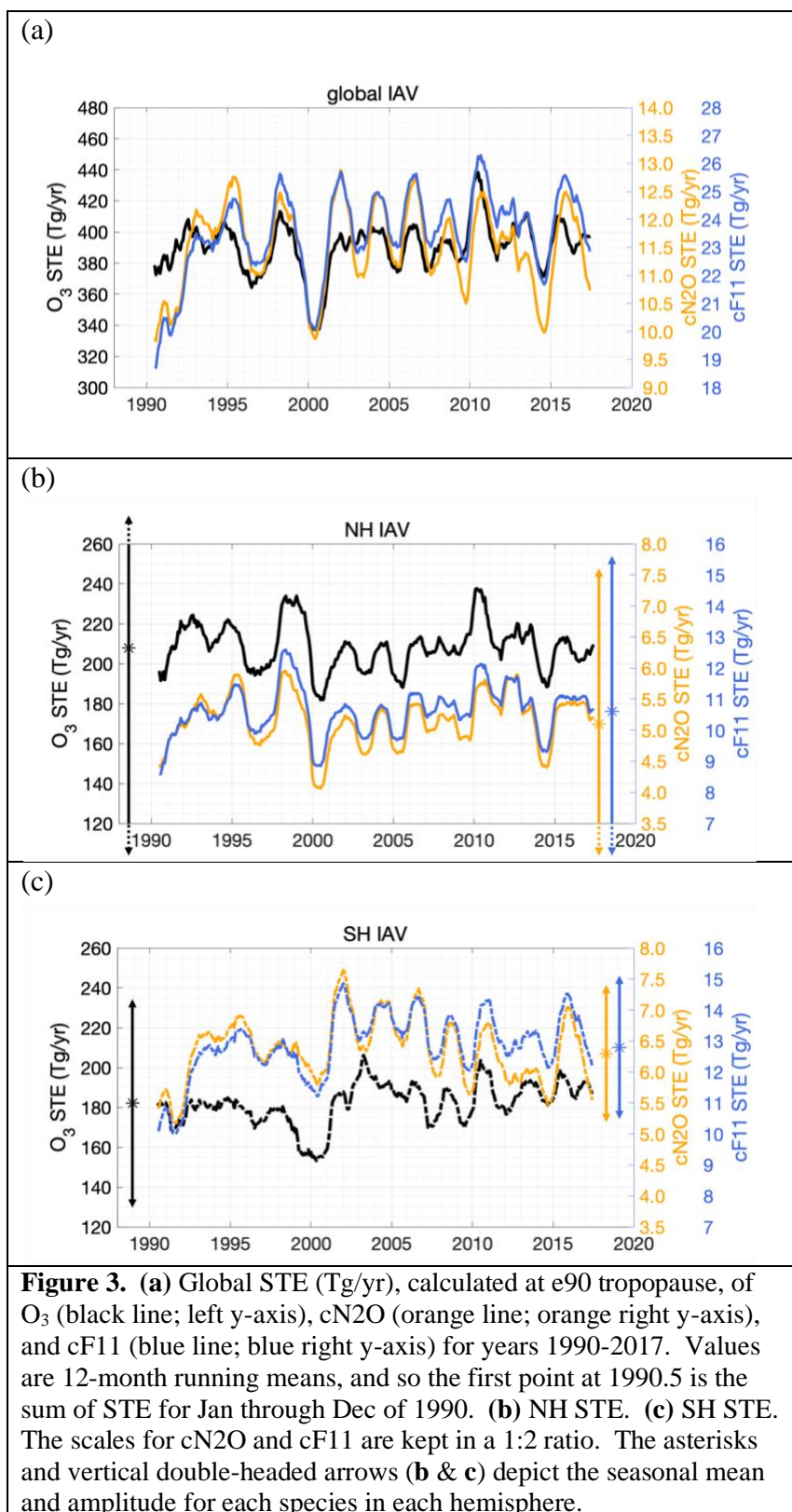
observed surface variability of N₂O from this circulation can be modeled and has a clear QBO signal, but one that is not strongly correlated with the QBO signal in stratospheric loss.

We generate the IAV of STE fluxes for O₃, cN₂O, and cF11 in Figure 3abc with panels for global, NH, and SH. Values are 12-month running means, and so the first modeled point at 1990.5 is the sum of STE for Jan through Dec of 1990. In Figures 3bc, we also show the seasonal amplitude of STE with double-headed arrows on the left (O₃) and right (cN₂O and cF11). In a surprising result, the large NH-SH differences in seasonal amplitude are not reflected in the IAV where NH and SH amplitudes are similar for all three tracers. The QBO modulation of the lowermost stratosphere and STE appears to be unrelated to the seasonal cycle in STE.

Global STE for all three tracers shows QBO-like cycling throughout the 1990-2017 time series: cN₂O and cF11 are well correlated ($cc \sim 0.9$), but either species with O₃ is much less so ($cc < 0.7$). The hemispheric breakdown provides key information regarding O₃. In the NH the STE IAV is similar across all three tracers with high correlation coefficients ($cc = 0.82$ for O₃-cN₂O, 0.83 for O₃-cF11, and 0.94 for cN₂O-cF11). Conversely in the SH, O₃ STE diverges from the c-tracer fluxes, showing opposite-sign peaks in 2003 and 2016. The corresponding SH correlations are ($cc = 0.38, 0.65, 0.85$). The loss of correlation between cN₂O and cF11 is unusual: cN₂O STE drifts downward relative to cF11 STE, particularly after 2007; nevertheless, the fine structure after 2007 is well matched in both tracers.

In the SH, the massive loss of O₃ within the Antarctic vortex, when mixed with the extra-polar lowermost stratosphere will systematically shift the O₃ STE to lower values, with less impact on the cN₂O and cF11 STE. The IAV of the Antarctic winter vortex, in terms of the amount of O₃ that is depleted (see Fig. 4-4 of WMO, 2018), appears to drive the decorrelation of the SH STE fluxes and is analyzed in section 4.

In the NH, the high variability of the Arctic winter stratosphere can modulate the total O₃ STE flux (e.g., Hsu and Prather, 2009) but appears to maintain the same relative ratio with the cN₂O and cF11 fluxes. Model results here indicate that in the NH, the IAV of O₃, cN₂O, and cF11 STE fluxes are synchronized, and thus the air masses entering the lowermost stratosphere have the same chemical mixtures from year to year. We know that cold-temperature activation of halogen-driven O₃ depletion in the Arctic winter at altitudes above 400 K (potential temperature) can produce large IAV in column ozone (Manney et al., 2011); but the magnitude is still much smaller than in the Antarctic; and it may not reach into the lowermost stratosphere (<380K potential temperature). This model accurately simulates Antarctic O₃ loss (section 4), but we have not evaluated it for Arctic loss, and the Arctic conditions operate closer to the thresholds initiating loss where Linoz v3 chemistry may be inadequate. The same meteorology and transport model with full stratospheric chemistry is able to simulate Arctic O₃ loss (Oslo's CTM2: Isaksen et al., 2012), and thus it will be possible to re-evaluate the NH IAV with such models or with lowermost stratosphere tracer measurements.



268
269

3.4 The link from stratospheric loss to STE flux

What is unusual about the very tight correlation of cN₂O and cF11 STE fluxes is that the photochemical loss of N₂O and F11 occurs at very different altitudes in the tropical stratosphere, which are not in phase with respect to the QBO as shown in R2021 (their Fig. 2). The separate phasing of cN₂O and cF11 production is lost, presumably by diffusive tracer transport, by the time they reach the extratropical lowermost stratosphere. The overall synchronization of the STE fluxes implies that the absolute STE flux is driven primarily by variations in venting of the lowermost stratosphere as expected (Holton et al., 1995; Appenzeller et al., 1996) rather than by variations in the chemistry of the middle stratosphere.

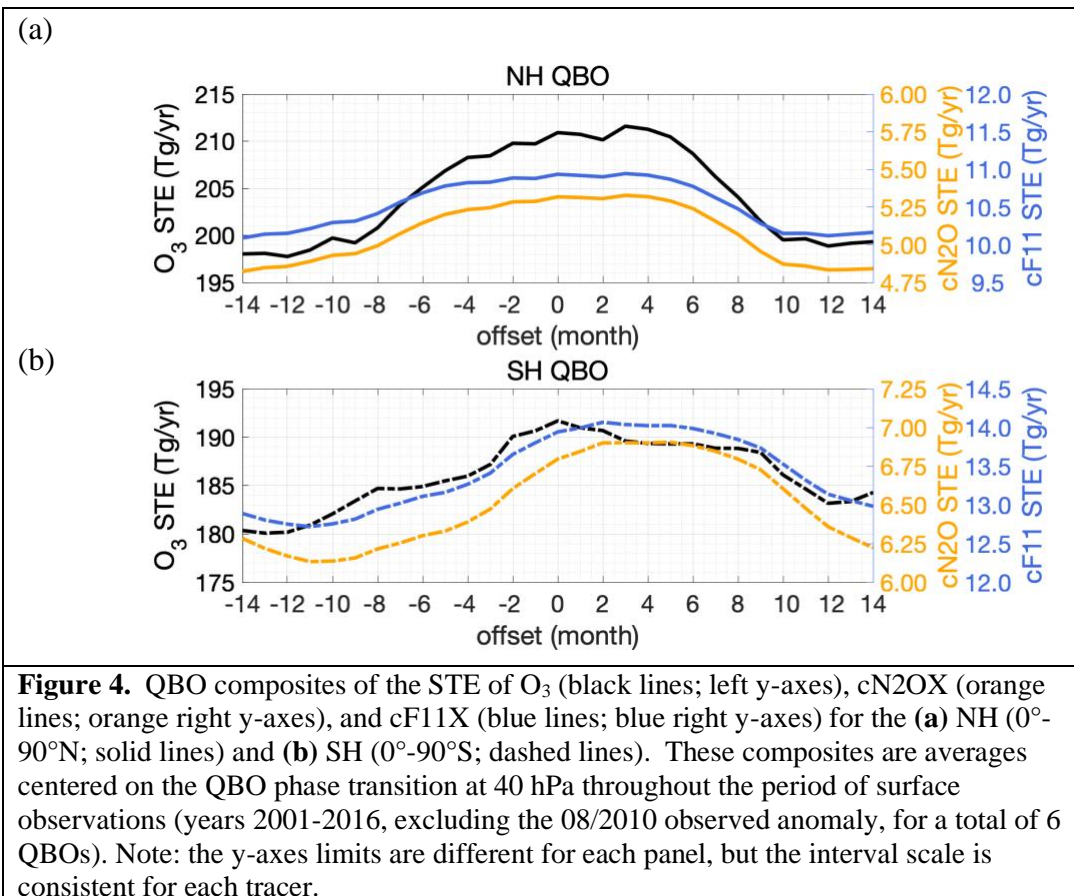
This disconnect between the chemical signals generated by the prominent QBO signature of wind reversals, upwelling in the tropical stratosphere, and the STE fluxes is also clear in the magnitude of the loss versus STE. For N₂O, the IAV of cN₂O production has a range of ± 0.5 Tg/yr, whether from Microwave Limb Sounder (MLS) observations or the model; whereas the IAV of cN₂O STE flux is ± 1.1 Tg/yr. The same is true in relative terms for cF11. Thus, the modulation of the lowermost stratosphere by the QBO is clearly a part of the overall changes in stratospheric circulation related to the QBO (Tung and Yang, 1994a; Kinnersley and Tung, 1999) and is the dominant source of IAV for these three greenhouse gases.

3.5. The QBO signal

To examine the QBO cycle in STE flux, we build a composite pattern (see R2021, Fig. 3 of N₂O surface variations), by synchronizing the STE IAV in Figure 2 with the QBO cycle. The sync point (offset = 0 months) is taken from one of the standard definitions of the QBO phase change, i.e., the shift in sign of the 40-hPa tropical zonal wind from easterly to westerly (Newman, 2020). The 1990-2017 model period has 12 QBO cycles, but we restrict our analysis here to years 2001-2016 to overlap with the observed surface N₂O data. This period includes seven QBO phase transitions (01/2002, 03/2004, 04/2006, 04/2008, 08/2010, 04/2013, 07/2015), but the observed surface N₂O is highly anomalous during the QBO centered on 08/2010 (R2021), so we remove it from our comparison for consistency with R2021 (see their Fig S4d). The resulting QBO composites for NH and SH in Figure 4 span 28 months.

In the NH, the QBO modulation of all three tracers is similar: STE flux begins to increase at an offset of -8 months and continues to increase slowly for a year, peaking at an offset of +4 months; thereafter it decreases more rapidly in about $\frac{1}{2}$ year (offset = +10). The rise-and-fall cycle takes about 18 months. In the SH, the pattern for cN₂O and cF11 is more sinusoidal and is shifted later by ~ 3 months. The SH amplitude of the c-tracers is slightly larger relative to the hemispheric mean flux than in the NH, and thus the SH QBO signal is larger than the NH by about 40%. Thus, over the typical QBO cycle centered on the sync point, more depleted N₂O and F11 is entering the SH than in the NH. For O₃, the SH modulation of STE is irregular and reduced compared with the NH. Our hypothesis here, consistent with the annual cycle of STE (Figure 1), is that the breakup of the Antarctic ozone hole has a major impact on STE, particularly that of O₃, and that its signal has large IAV that does not synchronize with the QBO. Surprisingly, the large wintertime IAV in the NH Arctic, in the form of sudden stratospheric warmings, does not seem to have a major role in STE fluxes as noted above. This model may

miss some of the Arctic O₃ depletion, but it accurately simulates the warmings, which must have a small impact on STE because they do not disrupt the clear QBO signal in the c-tracers.



4. Surface variability of N₂O related to STE flux

Surface variability of N₂O is driven by surface emissions, stratospheric loss, and atmospheric transport that mixes the first two signals. R2021 explored the variability originating only from stratospheric chemistry using the decaying tracer N2OX. Here, we use surf-N2O to denote the surface abundances of N2OX when corrected to steady state. R2021 showed that three independent chemistry-transport models produced annual and QBO patterns in surface N₂O simply from stratospheric loss. In this paper we link surf-N2O to the STE cN2O flux, which is linked above to the STE O₃ flux.

The observed surface N₂O, denoted obs-N₂O and taken from the NOAA network (Dlugokencky et al., 2019), shows a slowly increasing abundance (~0.9 ppb/yr) with a clear signal of annual and interannual variability at some latitudes (see R2021). We calculate annual and QBO-composite obs-N₂O after de-trending and restrict analysis in this section to model years 2001-2016 to be consistent with the surface data. The latitude-by-month pattern of obs-N₂O includes the impact of both stratospheric loss (~13.5 Tg/yr) and surface emissions (~17 TgN/yr), with the preponderance of emissions being in the NH (Tian et al., 2020). Total emissions are not

expected to have large IAV but may have a seasonal cycle. The seasonal variation of surface N₂O can also be driven by seasonality in the interhemispheric mixing of the NH-SH gradient (~1 ppb).

4.1 Annual cycle

Figure 5 replots the hemispheric mean annual cycles of cN₂O STE flux alongside the annual cycles of surf-N₂O and obs-N₂O. As noted above, the STE in each hemisphere is almost in opposite phase, as is the modeled surf-N₂O (taken from Fig. 5 of R2021). The NH:SH amplitude ratio is about 2.4:1 for both STE and surf-N₂O. The lag from peak STE flux of cN₂O (negative N₂O) to minimum surf-N₂O is about 3 months. Such a 90° phase shift is expected for the seasonal variation of a long-lived tracer relative to a seasonal source or sink. The time lag between the signal at the tropopause and at the surface, the tropospheric turnover time, should be no more than a month. Surprisingly, the cN₂O STE seasonal amplitude is much larger in the NH (±3.4 Tg/yr) than in the SH (±1.3 Tg/yr), although the SH mean (6.5 Tg/yr) is larger than the NH (5.2 Tg/yr). Essentially, there is more variability of air depleted in N₂O entering the NH, but air entering the SH has a larger overall deficit. Thus in our model, the stratosphere creates a NH-SH gradient of +0.3 ppb at the surface, which is a significant fraction of the observed N-S difference of +1.3 ppb (R2021). This important result needs to be verified with other models or analyses because it constrains the NH-SH location of sources.

In the NH, as noted in R2021, the two surface abundances, surf-N₂O and obs-N₂O, have the same amplitude and phase, implying that, if the model is correct, the emissions-driven surface signal has no seasonality, although we know that some important emissions are seasonal (Butterbach-Bahl et al., 2013). In the SH, the surf-N₂O signal is much smaller, in parallel with the small seasonal amplitude in cN₂O STE, but it is out of phase with the obs-N₂O. This result implies that the SH has some highly seasonal sources, or simply that the forcing of SH surf-N₂O by the seasonal cycle of cN₂O is weak. Indeed, this is what we might expect from Figure 3: In the NH the seasonal amplitude in N₂O overwhelms the IAV amplitude and is driving the obs-N₂O; but in the SH, both amplitudes are comparable. Given the quasi-regular nature of the QBO, it would interfere with the seasonal cycle and likely change its phase (as found for other models in R2021).

In the NH, the annual cycle of O₃ and cN₂O STE are clearly linked. If we accept that the obs-N₂O NH seasonal cycle is simply driven by the STE flux, then how will tropospheric O₃ respond seasonally? A mole-fraction scaling of the STE fluxes gives an O₃:N₂O ratio of ~25, and thus scaling the surf-N₂O amplitude gives a large O₃ surface seasonality of ~18 ppb. However, the residence time of a tropospheric O₃ perturbation is ~1 month, and thus the peak surface abundance will lag the peak STE flux by only about a month and not by 3 months as for N₂O. O₃ will equilibrate with the flux on monthly timescales and not accumulate. Thus, our estimate is that NH 30°-90° surface ozone might increase about 5 ppb, peaking in June, due to the STE flux. In the SH, seasonal patterns are weaker and not well defined, and thus no obvious STE O₃ signal is expected.

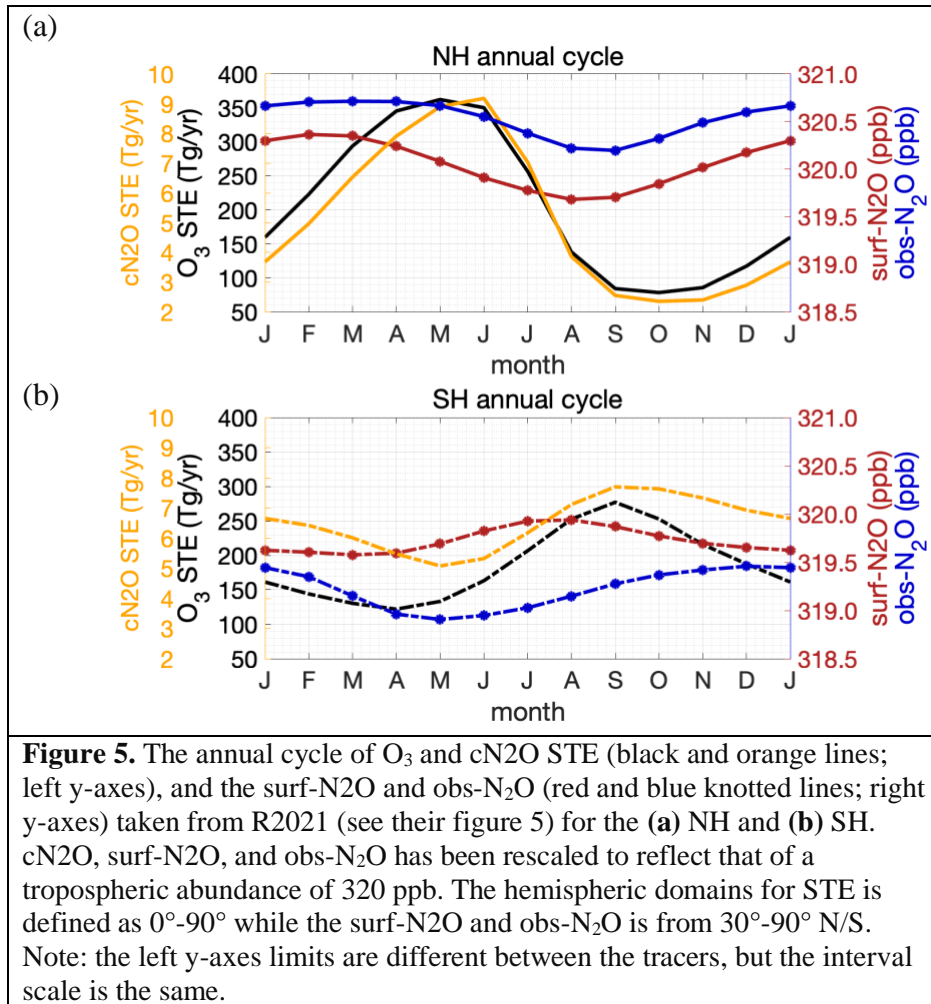


Figure 5. The annual cycle of O₃ and cN₂O STE (black and orange lines; left y-axes), and the surf-N₂O and obs-N₂O (red and blue knotted lines; right y-axes) taken from R2021 (see their figure 5) for the (a) NH and (b) SH. cN₂O, surf-N₂O, and obs-N₂O has been rescaled to reflect that of a tropospheric abundance of 320 ppb. The hemispheric domains for STE is defined as 0°-90° while the surf-N₂O and obs-N₂O is from 30°-90° N/S. Note: the left y-axes limits are different between the tracers, but the interval scale is the same.

4.2. QBO cycle

The QBO composite of hemispheric mean cN₂O STE flux from Figure 4 is compared with the composite of surface abundances (surf-N₂O and obs-N₂O) in Figure 6. The peak in cN₂O flux is broad and flat, but centers on +2 months for the NH and +4 months for the SH. Unlike the annual cycle, the QBO cycle in STE flux is almost in phase in both hemispheres, with the NH preceding the SH. This phasing of the QBO cycle in surface N₂O was seen with the three models in R2021. In both hemispheres, the modeled surf-N₂O peaks before the rise in cN₂O and then decreases through most of the period with elevated cN₂O flux as expected. The amplitude of the QBO STE flux is smaller in the NH than SH by about half, and the amplitude of surf-N₂O is likewise smaller. The ratio of the amplitudes of surf-N₂O to cN₂O STE flux is similar in both hemispheres (~ 0.4 ppb per Tg/yr), which is encouraging. This ratio is larger than the corresponding one from the annual cycles (~ 0.1 ppb per Tg/yr) because the length of the QBO cycle leads to longer accumulation of N₂O-depleted air from the cN₂O flux.

In the SH, where the QBO cycle in cN₂O flux has a large amplitude, the modeled surf-N₂O matches obs-N₂O in amplitude and phase as reported in R2021. In the NH, the comparison of

surf-N₂O with obs-N₂O is not so good: obs-N₂O has a much smaller amplitude and a different phase. This QBO cycle pattern is similar, but reversed, to that of the annual cycle and can be understood in the same way. The NH QBO cycle has relatively small amplitude and thus the interference with the large-amplitude annual cycle adds noise, obscuring the QBO cycle. In the SH it is the opposite, with its weak annual cycle, the SH QBO cycle is clear. The modeled cN₂O fluxes enable us to understand the large-scale variability of the observations.

Thus, for both annual and QBO fluctuations, when the variation in STE flux is dominated by either cycle, the surface variations are clearly seen and modeled for that cycle. This further supports the findings in R2021 and other studies, that hemispheric surface N₂O variability is driven by stratospheric loss on annual (NH) and QBO (SH) cycles, and it is clearly tied to the STE flux. Given the connection between O₃ and cN₂O STE, this relational metric can be used to constrain the O₃ STE for a model ensemble.

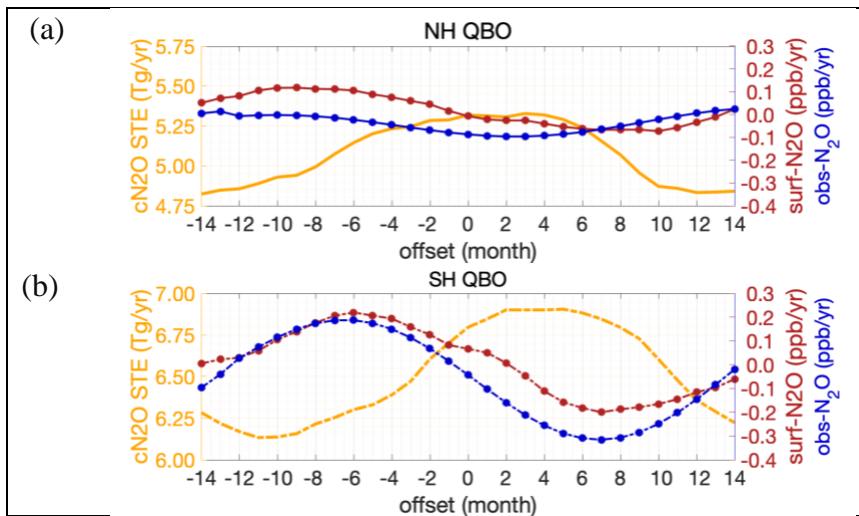


Figure 6. (a) NH and (b) SH QBO composites of cN₂O STE flux (Tg/yr; orange lines, left axis, Fig. 4), and surf-N₂O and obs-N₂O (ppb; red and blue knotted lines, right axes, see Fig. 3 of R2021). Results are shown for years 2001-2016 (6 QBO phase transitions), see Fig. 4. The surf-N₂O data is from UCI CTM, and obs-N₂O are taken from NOAA ESRL, see text.

5. Lowermost stratosphere

If we accept that matching the observed annual and QBO cycles in surface N₂O constrains the modeled STE cN₂O flux, then how can we use that to also constrain the modeled STE O₃ flux? All evidence, theoretical, observational, and modeled, shows that the STE flux is simultaneous for all species (e.g., Figure 1) and in proportion to their relative abundances (i.e., tracer:tracer slopes) in the lowermost stratosphere, defined roughly as the region 100-200 hPa in each hemisphere outside the tropics (Plumb and Ko, 1992).

5.1. The O₃:N₂O slopes and STE fluxes

We can test the Plumb and Ko hypothesis in our model framework by comparing the relative STE fluxes for O₃, cN₂O and cF11 with the modeled tracer-tracer slopes in the lowermost stratosphere. These slopes can then be tested using SCISAT-1 ACE-FTS (Scientific Satellite-1 Atmospheric Chemistry Experiment-Fourier Transform Spectrometer) measurements of O₃ and N₂O in the lowermost stratosphere to establish the ratio of the two STE fluxes.

Figure 7ab shows the N₂O-O₃ slope in each hemisphere taken from the ACE climatology dataset and the UCI CTM. The current ACE dataset (version 3.5) has been curated from measurements made by ACE-FTS from February 2004 to February 2013 (Koo et al., 2017). The SCISAT orbit results in irregular season-latitude coverage, and thus we average the lowermost stratosphere data over a wide range of latitudes centered on the peak STE flux (20°-60° in both hemispheres). For both ACE data and the CTM we keep to the lowermost stratosphere (200-100 hPa) and average over the 4-month peak of STE flux, Feb-May in the NH and Sep-Dec in the SH (see Figure 1). Extending into the upper tropical troposphere at 20° helps define the tropospheric end-point of the slope (low O₃, high N₂O).

Based on the long-term mean STE fluxes in the model, we would expect an O₃:N₂O slope of about -24 (ppb/ppb) in the NH and -17 in the SH. The slopes fitted to our modeled grid-cell values of O₃ and N₂O in the lowermost stratosphere are remarkably similar: -23.2 (NH) and -17.5 (SH). The ACE data are more scattered but show similar, smaller slopes of -19.4 (NH) and -15.3 (SH). Thus, the NH-SH asymmetry in O₃ versus N₂O STE fluxes is clearly reflected in the tracer-tracer slopes, both modeled and observed. Hegglin and Shepherd (2007) had already identified these NH:SH differences when comparing their model to the ACE-FTS observations (their Fig. 13cd), but implications for STE fluxes were not brought forward.

In the modeled SH (Figure 7b), one can see strings of points that are samples along neighboring cells and reflect a linear mixing line between two different end points, one of which has experienced extensive O₃ depletion (i.e., the Antarctic O₃ hole). We know that there is some chemical loss of O₃ in the NH lowermost polar stratosphere during very cold winters (Manney et al., 2011; Isaksen et al., 2012), but it is not extensive enough to systematically affect the O₃:N₂O slope over the mid-latitude lowermost stratosphere in either the ACE observations or the CTM simulations.

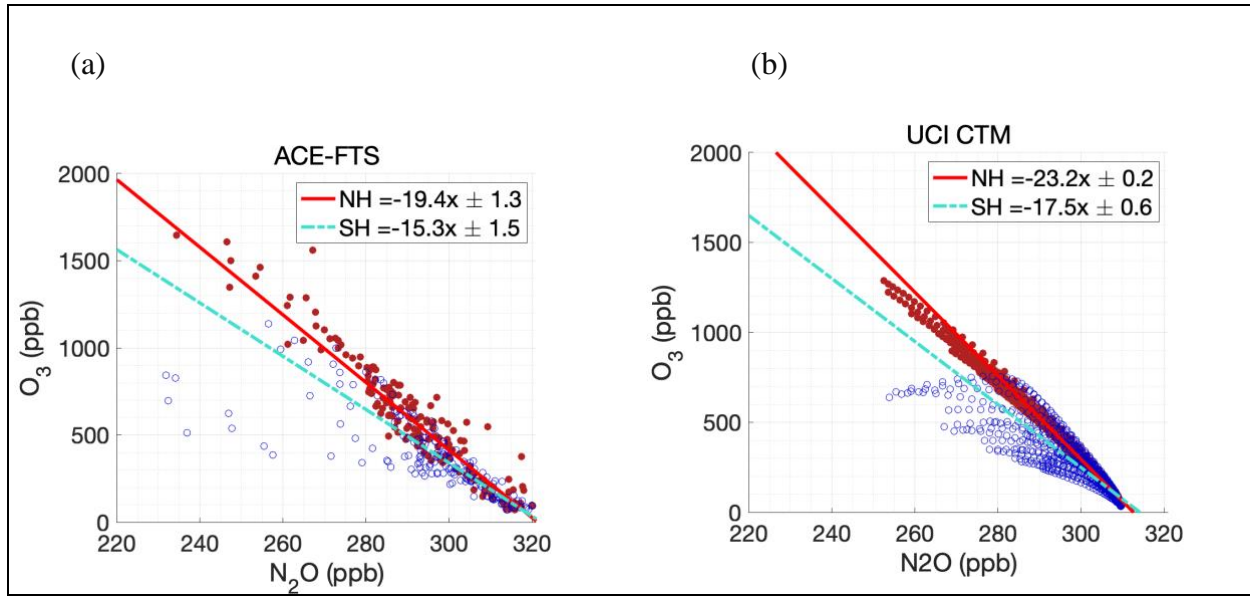


Figure 7. O₃ versus N₂O (x-axis) scatter plots from (a) SCISAT ACE-FTS and (b) the UCI CTM. ACE-FTS data is from monthly climatologies for the period Feb 2004 to Feb 2013 restricted to 200–100 hPa, latitudes about 20°–60°, and months Feb–May (NH, red) or Sep–Dec (SH, blue). The linear-fit lines (ppb/ppb, values in legend) are restricted to larger N₂O values (>280 ppb) to more accurately represent the STE fluxes, see Olsen et al. (2001).

5.2. IAV of the Antarctic ozone hole and the SH STE O₃ flux

The Antarctic ozone hole appears to be the source of the NH-SH asymmetry in the STE fluxes of O₃ versus N₂O. It is known that the massive chemical depletion of O₃ inside the Antarctic vortex between about 13 and 23 km altitude creates an air mass with lower O₃:N₂O ratios than usually found in the mid-latitude lowermost stratosphere. When the vortex breaks up, nominally in late November, much of this O₃-depleted air can mix along isentropes into the mid-latitude lowermost stratosphere, changing the O₃:N₂O ratios and reducing the SH STE O₃ flux.

We have additional information on the SH O₃ STE flux from the year-to-year variations in the size of the ozone hole. The best measure of the scale of Antarctic ozone depletion is the October mean ozone column (DU) averaged from the pole to 63°S equivalent latitude (see Fig. 4-5 of WMO, 2018). When we compare the CTM with the observations (Figure 8), we find remarkable verisimilitude in the model: the root-mean-squared difference is 9 DU out of a standard deviation of 29 DU and the correlation coefficient is 0.96. Thus, we have confidence that we are simulating the correct IAV of the ozone hole. Next, we plot the modeled O₃ STE flux (summed over the 12 months following the peak ozone hole, November–October) with the modeled October ozone column and find a fairly linear relationship. If we estimate the STE O₃ flux before the O₃ hole, when the mean October O₃ column was about 307 DU, then our O₃ flux increases to 209 Tg/yr (see Figure 8, red marker), eliminating the hemispheric asymmetry in O₃ STE flux.

The annual deficit in SH STE O₃ flux brought on by the Antarctic ozone hole ranges from about 5 to 55 Tg/yr and with a central value of 30 Tg/yr or 14% of the total. Using the decadal trends

1965-2000 from Hegglin and Shepherd (2009), this deficit is 8%; and from Meul et al. (2018), 5%. Since both of these models calculate a much larger SH flux (~300 Tg/yr), we estimate their absolute change in O₃ flux to be 24 and 15 Tg/yr, respectively. Because the ozone hole effectively removes a fixed, rather than proportional, amount of ozone that presumably is mapped onto the STE flux the following year, we believe the absolute change is the best measure. Thus the three models estimate the ozone hole causes a deficit in the SH O₃ STE flux in the range of 15-30 Tg/yr. The UCI CTM's ability to match the observed IAV of the ozone hole, and to match that linearly with the deficit in STE flux provides support for the upper end of the range. Note that the difference in O₃:N₂O slopes between NH and SH in Figure 7 is about 5. If we attribute that solely to the ozone hole and split the flux of N₂O-depleted air evenly between hemispheres, then the ozone-hole-driven O₃ STE flux difference is about 55 Tg/yr, about twice that derived from the variability in our model. This difference in estimated flux indicates that even without chlorine-driven ozone depletion, the O₃:N₂O slopes may be inherently different simply because of the strong descent inside the wintertime Antarctic vortex. This can be readily investigated with further model studies.

We looked for any relationship between ozone hole IAV and the STE fluxes of cN₂O or cF11 and found mostly a scatter plot with no clear relationship. Given the analysis above, we expect that much of the scatter is related to QBO cycles.

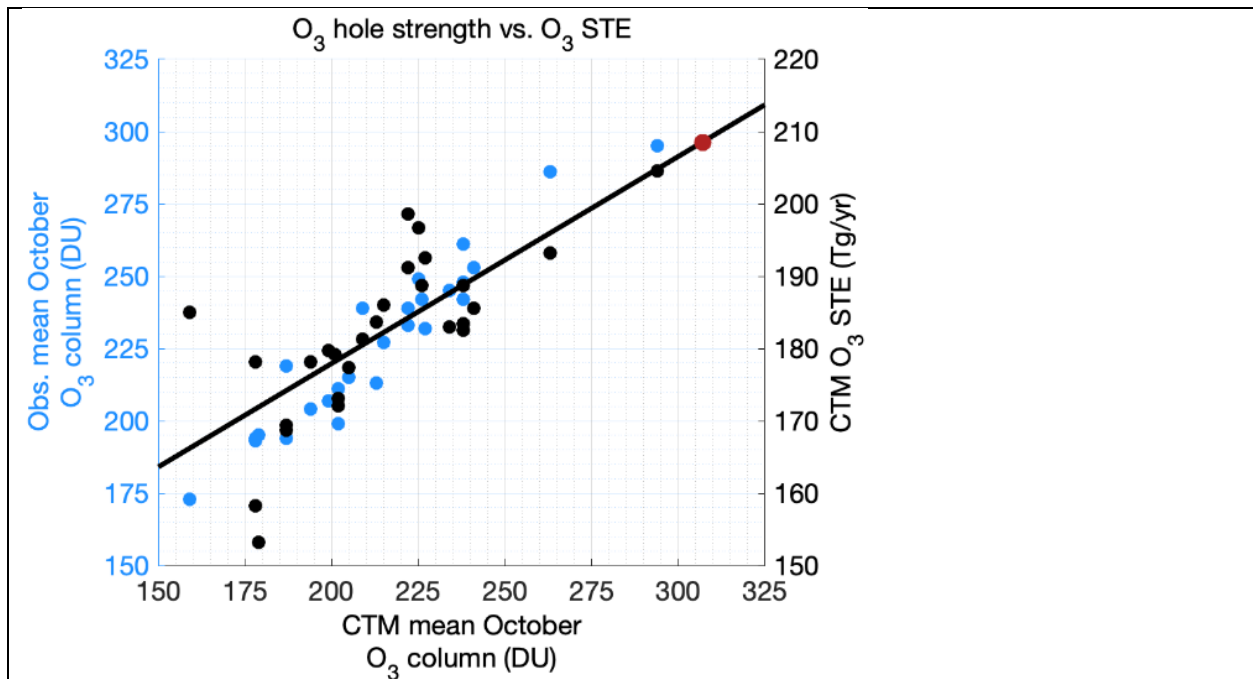
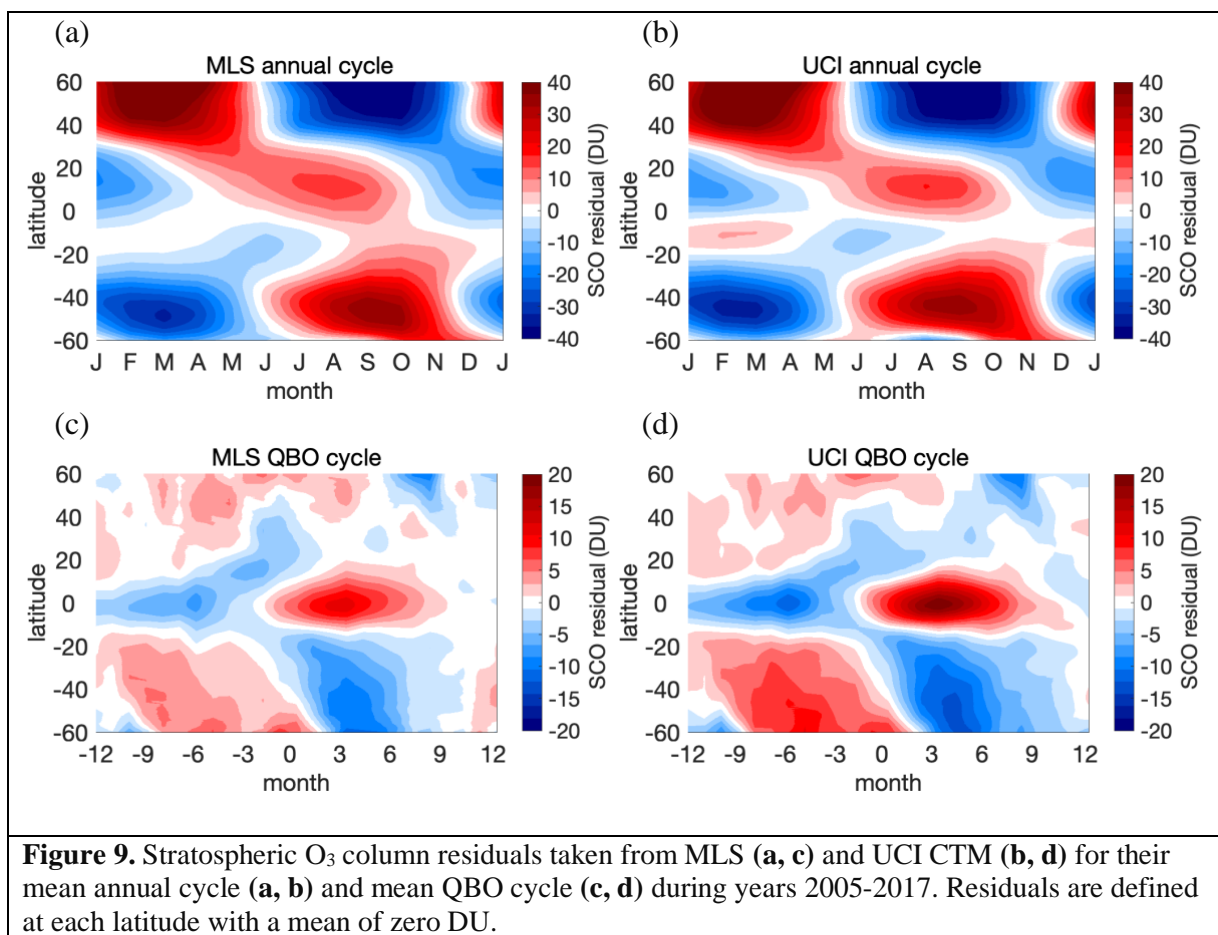


Figure 8. Interannual variability of the observed Antarctic ozone hole from 1990 to 2017 (blue dots; left y-axis) versus the CTM modeled ozone hole (x-axis); plus the CTM modeled SH STE O₃ flux (black dots; right y-axis) versus the modeled ozone hole (x-axis). The ozone hole is measured by the total ozone column (DU) averaged daily over October poleward of 63°S in equivalent latitude (see Figure 4.5 of WMO 2018). The SH STE O₃ flux (Tg/yr) is centered on May 1 of the following year (i.e., the 12 months following the nominal breakup of the ozone hole). The black line is a simple regression fit of the modeled STE to the modeled ozone hole (black dots), and the red dot is our estimate of pre-ozone-hole SH STE O₃ flux based on the observed 1979-82 O₃ column.

5.3 Other model-measurement metrics related to STE

What else might affect O₃ STE? Stratospheric column O₃ (DU) varies on annual and QBO timescales. These changes in O₃ overhead can have a direct influence on O₃ transport to the troposphere, but the link requires further analysis. Tang et al. (2021) showed the UCI CTM is able to capture the observed annual cycle of stratospheric O₃ column as extracted from total column using the Ziemke et al. (2019) method. QBO modulation of stratospheric column O₃ has not been fully investigated since Tung and Yang (1994b). Yet, the fluctuations in mass over the annual cycle are comparable to the corresponding variability in O₃ STE flux (1 DU = 10.9 Tg) and likely connected (Figure 9).



6. Conclusions

This work examines how closely O₃ STE is linked to STE fluxes of other trace gases. By including our complementary N₂O and F11 tracers, we can follow stratospheric loss of these gases along with stratospheric O₃ across the tropopause. The magnitudes of the fluxes are proportional to their abundances in the lower stratosphere as expected (Plumb and Ko, 1992),

and their variability is highly correlated with one another, indicating that they are entering the troposphere simultaneously. Even the distinct QBO pattern of STE fluxes is consistent across O₃, N₂O and F11. We further constrain the N₂O transport pathway by linking STE of depleted-N₂O air with surface fluctuations of N₂O abundance. The surface response in modeled N₂O matches well with the observed surface variability in the SH, indicating that surface variability is driven largely by STE flux.

Consistency of STE O₃ flux. As summarized here, there are a number of model diagnostics and observational constraints that provide a reality check on the consistency of the modeled O₃ STE flux. In Table 1, we examine these for our model and also for the CMAM model (Hegglin and Shepherd, 2007, 2009) because it is one of the few with enough published results. For UCI we calculate NH:SH fluxes of O₃ (208:182 Tg-O₃/yr) and N₂O (5.1:6.4 Tg-N/yr). Thus the mole fraction slopes in the lowermost stratosphere should be -23.8 (NH) and -16.6 (SH). Our model O₃:N₂O slopes are -23.2 (NH) and -17.5 (SH). Given the seasonal variability and scatter in the correlation plots (Figure 7), we count this as consistent. For CMAM, the modeled O₃:N₂O slopes, -21 (NH) and -18 (SH) are similar to ours and to the ACE-FTS observations as analyzed by Hegglin and Shepherd (2007), -22 (NH) and -15 (SH), or by us, -19 (NH) and -15 (SH). CMAM does not report the STE N₂O fluxes, but their model seems to match observations and so we assume that the MLS-derived N₂O fluxes are a close estimate (12.9 Tg-N/yr). Just using the CMAM global numbers for O₃ STE flux, we calculate the O₃:N₂O slope in the lowermost stratosphere should average to -30. We conclude that their diagnosis of the STE O₃ flux, 655 Tg/yr, is inconsistent with the circulation that generated the O₃:N₂O slopes and is 50% too large. We do not view this as a critical assessment of CMAM since it involves us combining diagnostics from two separate publications, but it is an example of how we might expect future studies of the STE O₃ flux to self-evaluate.

Uncertainty Quantification in STE O₃ flux. Deriving a best estimate and uncertainty from this work involves expert judgment. Changes in meteorological data used by the UCI CTM (IFS Cycles 29r1, 36r1, and 38r1, all at 60-layer 1.1° resolution, see Table 1) give a standard deviation in STE of 13% (only 3 values). If we use observations to derive a value as in Murphy and Fahey (1994), we must expand our dimensions to the uncertainty in the NH:SH split of N₂O flux to calculate each hemisphere's O₃ flux. The factors are: (1) total STE N₂O flux is 12.9 Tg-N/yr from the MLS data and we assign a ±10% one-sigma uncertainty; (2) the NH:SH split of the N₂O flux is 44:56 in our current model, was not diagnosed for previous ones, and so we assume a value of 50:50 that ranges from 40:60 to 60:40; (3) analysis of the ACE-FTS observations (ours and Hegglin and Shepherd, 2007) gives O₃:N₂O slopes of about -21 (NH) and -15 (SH) to which we assign a one-sigma uncertainty of ±3. Propagating these as root-mean square errors, we find a ±15% uncertainty in the global value, 400 ± 60 Tg/yr. Uncertainty in the hemispheric values is more difficult to assess, and from a range of model results shown in Table 1, we can only estimate that the NH:SH ratio is between 60:40 and 50:50, a range that bounds our and CMAM results plus 2%. Note that this estimate is for current conditions with a regularly occurring Antarctic ozone hole. We believe the low 50:50 ratio is plausible because we have shown that our large SH STE N₂O flux is consistent with the surface QBO variability in N₂O. For pre-1980, and for when the ozone hole recovers later this century, we anticipate that the SH O₃:N₂O slope will revert to -18 to -21, and the total STE O₃ flux to 430-460 Tg/yr. This simplistic estimate is based on a fixed atmospheric circulation.

A major surprise from our model is that the STE flux of O₃ is predominantly NH biased currently, only because of the Antarctic ozone hole. Prior to 1980, and after 2060, it would/will be symmetric between the hemispheres. Our model calculates slightly greater STE fluxes for trace gases like N₂O or F11 in the SH, which is counter to prevailing theory that the wave-driven fluxes force relatively greater STE in the NH. This difference cannot be directly tested with observations of trace gases, but a range of N₂O hemispheric observations are well modeled and support this premise. More extensive work with multi-model ensembles that include both chemical and dynamical diagnostics in the stratosphere would be needed to overturn the established theory. Our work reemphasizes the importance of trace-gas correlations in the lowermost stratosphere as a key observational metric for climate models that may be able to constrain total STE fluxes. The tracer slopes may go beyond just relative STE fluxes because we have other measurements from the upper stratosphere to the surface that constrain, for example, the absolute flux of N₂O better than we first did using just the modeled lifetime.

In Table 2, we gather a set of observation-based model metrics that relate to STE fluxes and will help the community build more robust models to better derive the STE flux of O₃.

Table 1. Summary of key results for the STE flux of O ₃ and N ₂ O presented here (bold)				
	NH	SH	Global	notes
STE O ₃ flux (TgO ₃ /yr)	208	182	390	IFS Cy38r1, yrs 1990-2017 (this paper; Ruiz et al., 2021)
	239	198	437	IFS Cy36r1, yrs 2000-2007 (Hsu & Prather, 2014)
	301	233	534	IFS Cy29r1, yrs 2000-2006 (Hsu & Prather, 2014)
	383	272	655	CMAM, yrs 1995-2005 (Hegglin & Shepherd, 2009)
STE N ₂ O flux (TgN/yr)	5.1	6.4	11.5	yrs 1990-2017, scaled to 320 ppb
			12.9	using MLS lifetime of 119 yr and 320 ppb
LMS O ₃ :N ₂ O slope*	-23.2	-17.5		UCI model
	-19.4	-15.3		ACE-FTS observations
	-23.0	-17.5		CMAM model, Fig 13 of (Hegglin & Shepherd, 2007)
	-22.0	-15.0		ACE-FTS observations, ibid
			-20.0	(Murphy & Fahey, 1994)
			-22.0	(McLinden et al., 2000)
STE flux O ₃ :N ₂ O (mole/mole)	-23.8	-16.6		UCI model, calculated from entries above
			-29.6	CMAM (Hegglin & Shepherd, 2009), using MLS N ₂ O lifetime
Best Estimate STE O ₃ flux (Tg/yr)	60% to 50%	40% to 50%	400 ± 60	current Antarctic ozone hole conditions, see text
* LMS = lowermost stratosphere. For UCI model, months are selected for highest STE (FMAM in NH, SOND in SH, Fig. 1). For CMAM, annual averages from their Fig. 13cd. Where no reference is given, the source is this paper.				

Table 2. Metrics from Measurements or Constrained Values for CCMs related to Stratosphere-Troposphere Exchange				
<i>Name</i>	<i>Metric</i>	<i>Measured values</i>	<i>Model requirements</i>	<i>Example figure</i>
N ₂ O loss	Annual and QBO cycles of global mean stratospheric N ₂ O loss	Monthly N ₂ O loss calculated from MLS profiles (2005-present)	Stratospheric chemistry for N ₂ O as tracer; a QBO cycle; monthly mean diagnostics	Fig. 4 (Prather et al., 2015); Fig. 2 (Ruiz et al., 2021); Fig. 3 (this paper)
STE slopes	Matching O ₃ :N ₂ O slopes in lowermost stratosphere	ACE FTS profiles (2004-2013)	Stratospheric O ₃ and N ₂ O calculation, possibly also CFCs; monthly snapshots	Fig. 7 (this paper)
Strat O ₃ column	Annual and QBO composite cycles of stratospheric O ₃ column	Monthly zonal mean stratospheric O ₃ column from Ziemke et al., 2019 (2005-present)	Stratospheric O ₃ chemistry; a QBO cycle; monthly mean diagnostics; separate strat & trop O ₃ columns	Fig. 9 (this paper)
N ₂ O loss at surface	Annual and QBO composite cycles of surface N ₂ O solely from stratospheric loss	NOAA surface N ₂ O observations	Stratospheric N ₂ O chemistry; N ₂ OX as a tracer; monthly mean diagnostics	Fig. 3 (Ruiz et al., 2021); Fig. 5 (this paper)
		<i>Constrained (modeled) values</i>		
STE flux of O ₃		Monthly, latitude or hemispheric resolved, net O ₃ flux	Run O3strat as a tracer; diagnose monthly flux into troposphere, at tropopause or through trop- loss of O3strat	Fig. 1 & 2 (this paper)
STE flux of N ₂ O depleted air (also CFC-11)		Monthly, latitude or hemispheric resolved, STE flux of N ₂ O (CFC-11)	Run cN2O (cF11) as a tracer; diagnose monthly flux into troposphere	Fig. 1 & 2 (this paper);
SH O ₃ hole and flux		Change in SH O ₃ STE flux with size of ozone hole; observed IAV of O ₃ hole	IAV of ozone hole; daily total O ₃ column (lat, long); monthly SH O ₃ STE flux	Fig 7 (this paper)
Notes: Constrained values are model-only derived quantities that can be diagnosed from CCMs or CTMs.				

609
610
611
612
613
614
615
616
617
618
619
620
621
622
623
624

Author Contributions:

DJR and MJP designed and carried out the study and prepared the manuscript for publication.

Competing interests:

The authors declare that they have no conflict of interest.

Acknowledgments:

Research at UCI was supported by grants from the National Aeronautics and Space Administration's Modeling, Analysis and Prediction Program (award NNX13AL12G), and Atmospheric Chemistry Modeling and Analysis Program (80NSSC20K1237, NNX15AE35G), and the National Science Foundation (NRT-1633631). We gratefully acknowledge the work of the MLS team in producing the Level 3 data sets that enabled our MLS-related analyses. Work at the Jet Propulsion Laboratory, California Institute of Technology, was performed under contract with the National Aeronautics and Space Administration. We thank the ACE-FTS team for making the climatology data used here available for our analyses. The Atmospheric Chemistry Experiment (ACE), also known as SCISAT, is a Canadian-led mission mainly supported by the Canadian Space Agency. We also acknowledge Ed Dlugokencky for providing the surface N₂O data that was used here to produce an observation-based reference with which to compare our simulated results. The data used to produce the figures and tables in this work are accessible via the DRYAD repository with DOI <https://doi.org/10.7280/D1JX0K>

References:

- Appenzeller, C., Holton, J. R., and Rosenlof, K. H.: Seasonal variation of mass transport across the tropopause, *J Geophys Res-Atmos*, 101, 15071-15078, doi:10.1029/96JD00821, 1996.
- Baldwin, M. P., Gray, L. J., Dunkerton, T. J., Hamilton, K., Haynes, P. H., Randel, W. J., Holton, J. R., Alexander, M. J., Hirota, I., Horinouchi, T., Jones, D. B. A., Kinnnersley, J. S., Marquardt, C., Sato, K., and Takahashi, M.: The quasi-biennial oscillation, *Reviews of Geophysics*, 39, 179-229, 2001.
- Butterbach-Bahl, K., Baggs, E. M., Dannenmann, M., Kiese, R., and Zechmeister-Boltenstern, S.: Nitrous oxide emissions from soils: how well do we understand the processes and their controls?, *Philos T R Soc B*, 368, 10.1098/rstb.2013.0122, 2013.
- Dlugokencky, E. J., Crotwell, A. M., Mund, J. W., Crotwell, M. J., and Thoning, K. W.: Atmospheric Nitrous Oxide Dry Air Mole Fractions from the NOAA ESRL Carbon Cycle Cooperative Global Air Sampling Network, 1997-2018, Version: 2019-07, 10.15138/53g1-x417, 2019.
- Gettelman, A., Holton, J. R., and Rosenlof, K. H.: Mass fluxes of O-3, CH4, N2O and CF2Cl2 in the lower stratosphere calculated from observational data, *J Geophys Res-Atmos*, 102, 19149-19159, Doi 10.1029/97jd01014, 1997.
- Griffiths, P. T., Murray, L. T., Zeng, G., Shin, Y. M., Abraham, N. L., Archibald, A. T., Deushi, M., Emmons, L. K., Galbally, I. E., Hassler, B., Horowitz, L. W., Keeble, J., Liu, J., Moeini, O., Naik, V., O'Connor, F. M., Oshima, N., Tarasick, D., Tilmes, S., Turnock, S. T., Wild, O., Young, P. J., and Zanis, P.: Tropospheric ozone in CMIP6 simulations, *Atmos Chem Phys*, 21, 4187-4218, 10.5194/acp-21-4187-2021, 2021.
- Hamilton, K., and Fan, S. M.: Effects of the stratospheric quasi-biennial oscillation on long-lived greenhouse gases in the troposphere, *J Geophys Res-Atmos*, 105, 20581-20587, 10.1029/2000jd900331, 2000.
- Hegglin, M. I., and Shepherd, T. G.: Large climate-induced changes in ultraviolet index and stratosphere-to-troposphere ozone flux, *Nature Geoscience*, 2, 687-691, Doi 10.1038/Ngeo604, 2009.
- Hegglin, M. I., and Shepherd, T. G.: O3-N2O correlations from the Atmospheric Chemistry Experiment: Revisiting a diagnostic of transport and chemistry in the stratosphere, *J Geophys Res-Atmos*, 112, Artn D19301, 10.1029/2006jd008281, 2007.
- Hess, P., Kinnison, D., and Tang, Q.: Ensemble simulations of the role of the stratosphere in the attribution of northern extratropical tropospheric ozone variability, *Atmos Chem Phys*, 15, 2341-2365, 10.5194/acp-15-2341-2015, 2015.
- Hirsch, A. I., Michalak, A. M., Bruhwiler, L. M., Peters, W., Dlugokencky, E. J., and Tans, P. P.: Inverse modeling estimates of the global nitrous oxide surface flux from 1998-2001, *Global Biogeochem Cy*, 20, Artn Gb1008, 10.1029/2004gb002443, 2006.
- Holton, J. R., Haynes, P. H., McIntyre, M. E., Douglass, A. R., Rood, R. B., and Pfister, L.: Stratosphere-Troposphere Exchange, *Reviews of Geophysics*, 33, 403-439, 1995.
- Holton, J. R.: On the Global Exchange of Mass between the Stratosphere and Troposphere, *J Atmos Sci*, 47, 392-395, Doi 10.1175/1520-0469(1990)047<0392:Otgeom>2.0.Co;2, 1990.
- Hsu, J. N., and Prather, M. J.: Is the residual vertical velocity a good proxy for stratosphere-troposphere exchange of ozone?, *Geophys Res Lett*, 41, 9024-9032, 10.1002/2014GL061994, 2014.

Hsu, J., and Prather, M. J.: Global long-lived chemical modes excited in a 3-D chemistry transport model: Stratospheric N₂O, NO_y, O₃ and CH₄ chemistry, *Geophys Res Lett*, 37, L07805, Artn L07805, 10.1029/2009gl042243, 2010.

Hsu, J., and Prather, M. J.: Stratospheric variability and tropospheric ozone, *J Geophys Res-Atmos*, 114, Artn D06102, 10.1029/2008jd010942, 2009.

Hsu, J., Prather, M. J., and Wild, O.: Diagnosing the stratosphere-to-troposphere flux of ozone in a chemistry transport model, *J Geophys Res-Atmos*, 110, Artn D19305, 10.1029/2005jd006045, 2005.

Isaksen, I. S. A., Zerefos, C., Wang, W. C., Balis, D., Eleftheratos, K., Rognerud, B., Stordal, F., Bernsten, T. K., LaCasce, J. H., Sovde, O. A., Olivie, D., Orsolini, Y. J., Zyrichidou, I., Prather, M., and Tuinder, O. N. E.: Attribution of the Arctic ozone column deficit in March 2011, *Geophys Res Lett*, 39, Artn L24810, 10.1029/2012gl053876, 2012.

Kinnersley, J. S., and Tung, K. K.: Mechanisms for the extratropical QBO in circulation and ozone, *J Atmos Sci*, 56, 1942-1962, Doi 10.1175/1520-0469(1999)056<1942:Mfteqi>2.0.Co;2, 1999.

Koo, J. H., Walker, K. A., Jones, A., Sheese, P. E., Boone, C. D., Bernath, P. F., & Manney, G. L.: Global climatology based on the ACE-FTS version 3.5 dataset: Addition of mesospheric levels and carbon-containing species in the UTLS. *Journal of Quantitative Spectroscopy and Radiative Transfer*, 186, 52–62, 10.1016/j.jqsrt.2016.07.003, 2017.

Liang, Y. X., Gillett, N. P., and Monahan, A. H.: Climate Model Projections of 21st Century Global Warming Constrained Using the Observed Warming Trend, *Geophys Res Lett*, 47, ARTN e2019GL086757, 10.1029/2019GL086757, 2020.

Liu, H. Y., Considine, D. B., Horowitz, L. W., Crawford, J. H., Rodriguez, J. M., Strahan, S. E., Damon, M. R., Steenrod, S. D., Xu, X. J., Kouatchou, J., Carouge, C., and Yantosca, R. M.: Using beryllium-7 to assess cross-tropopause transport in global models, *Atmos Chem Phys*, 16, 4641-4659, 10.5194/acp-16-4641-2016, 2016.

Manney, G. L., Santee, M. L., Rex, M., Livesey, N. J., Pitts, M. C., Veefkind, P., Nash, E. R., Wohltmann, I., Lehmann, R., Froidevaux, L., Poole, L. R., Schoeberl, M. R., Haffner, D. P., Davies, J., Dorokhov, V., Gernandt, H., Johnson, B., Kivi, R., Kyro, E., Larsen, N., Levelt, P. F., Makshtas, A., McElroy, C. T., Nakajima, H., Parrondo, M. C., Tarasick, D. W., von der Gathen, P., Walker, K. A., and Zinoviev, N. S.: Unprecedented Arctic ozone loss in 2011, *Nature*, 478, 469-U465, 10.1038/nature10556, 2011.

McLinden, C. A., Olsen, S. C., Hannegan, B., Wild, O., Prather, M. J., and Sundet, J.: Stratospheric ozone in 3-D models: A simple chemistry and the cross-tropopause flux, *J Geophys Res-Atmos*, 105, 14653-14665, 10.1029/2000JD900124, 2000.

Meul, S., Langematz, U., Kroger, P., Oberlander-Hayn, S., and Jockel, P.: Future changes in the stratosphere-to-troposphere ozone mass flux and the contribution from climate change and ozone recovery, *Atmos Chem Phys*, 18, 7721-7738, 10.5194/acp-18-7721-2018, 2018.

Montzka, S. A., Dutton, G. S., Yu, P. F., Ray, E., Portmann, R. W., Daniel, J. S., Kuijpers, L., Hall, B. D., Mondeel, D., Siso, C., Nance, D., Rigby, M., Manning, A. J., Hu, L., Moore, F., Miller, B. R., and Elkins, J. W.: An unexpected and persistent increase in global emissions of ozone-depleting CFC-11, *Nature*, 557, 413-416, 10.1038/s41586-018-0106-2, 2018.

Murphy, D. M., and Fahey, D. W.: An estimate of the flux of stratospheric reactive nitrogen and ozone into the troposphere, *Journal of Geophysical Research*, 99, 5325-5332, 1994.

- Nevison, C. D., Kinnison, D. E., and Weiss, R. F.: Stratospheric influences on the tropospheric seasonal cycles of nitrous oxide and chlorofluorocarbons, *Geophys Res Lett*, 31, Artn L20103, 10.1029/2004gl020398, 2004.
- Nevison, C. D., Mahowald, N. M., Weiss, R. F., and Prinn, R. G.: Interannual and seasonal variability in atmospheric N₂O, *Global Biogeochem Cy*, 21, Artn Gb3017, 10.1029/2006gb002755, 2007.
- Newman, P.: The quasi-biennial oscillation (QBO), NASA, Goddard Space Flight Center, https://acd-ext.gsfc.nasa.gov/Data_services/met/qbo/qbo.html, retrieved on 3 Mar 2020.
- Olsen, M. A., Manney, G. L., and Liu, J. H.: The ENSO and QBO Impact on Ozone Variability and Stratosphere-Troposphere Exchange Relative to the Subtropical Jets, *J Geophys Res-Atmos*, 124, 7379-7392, 10.1029/2019JD030435, 2019.
- Olsen, M. A., Schoeberl, M. R., and Douglass, A. R.: Stratosphere-troposphere exchange of mass and ozone, *J Geophys Res-Atmos*, 109, Artn D24114, 10.1029/2004jd005186, 2004.
- Olsen, S. C., McLinden, C. A., and Prather, M. J.: Stratospheric N₂O-NO_y system: testing uncertainties in a three-dimensional framework, *J. Geophys. Res.*, 106, 28771-28784, 2001.
- Plumb, R. A., and Ko, M. K. W.: Interrelationships between Mixing Ratios of Long Lived Stratospheric Constituents, *J Geophys Res-Atmos*, 97, 10145-10156, 1992.
- Prather, M. J., Hsu, J., DeLuca, N. M., Jackman, C. H., Oman, L. D., Douglass, A. R., Fleming, E. L., Strahan, S. E., Steenrod, S. D., Sovde, O. A., Isaksen, I. S. A., Froidevaux, L., and Funke, B.: Measuring and modeling the lifetime of nitrous oxide including its variability, *J Geophys Res-Atmos*, 120, 5693-5705, 10.1002/2015JD023267, 2015.
- Prather, M. J., Zhu, X., Tang, Q., Hsu, J., and Neu, J. L.: An atmospheric chemist in search of the tropopause, *J. Geophys. Res.*, 116, D04306, 10.1029/2010jd014939, 2011.
- Ray, E. A., Portmann, R. W., Yu, P. F., Daniel, J., Montzka, S. A., Dutton, G. S., Hall, B. D., Moore, F. L., and Rosenlof, K. H.: The influence of the stratospheric Quasi-Biennial Oscillation on trace gas levels at the Earth's surface, *Nat Geosci*, 13, 22-24, 10.1038/s41561-019-0507-3, 2020.
- Ruiz, D. J., Prather, M. J., Strahan, S. E., Thompson, R. L., Froidevaux, L., and Steenrod, S. D.: How Atmospheric Chemistry and Transport Drive Surface Variability of N₂O and CFC-11, *J Geophys Res-Atmos*, 126, ARTN e2020JD033979, 10.1029/2020JD033979, 2021.
- Stohl, A., Bonasoni, P., Cristofanelli, P., Collins, W., Feichter, J., Frank, A., Forster, C., Gerasopoulos, E., Gaggeler, H., James, P., Kentarchos, T., Kromp-Kolb, H., Kruger, B., Land, C., Meloan, J., Papayannis, A., Priller, A., Seibert, P., Sprenger, M., Roelofs, G. J., Scheel, H. E., Schnabel, C., Siegmund, P., Tobler, L., Trickl, T., Wernli, H., Wirth, V., Zanis, P., and Zerefos, C.: Stratosphere-troposphere exchange: A review, and what we have learned from STACCATO, *J Geophys Res-Atmos*, 108, Artn 8516, 10.1029/2002jd002490, 2003.
- Strahan, S. E., Douglass, A. R., Stolarski, R. S., Akiyoshi, H., Bekki, S., Braesicke, P., Butchart, N., Chipperfield, M. P., Cugnet, D., Dhomse, S., Frith, S. M., Gettelman, A., Hardiman, S. C., Kinnison, D. E., Lamarque, J. F., Mancini, E., Marchand, M., Michou, M., Morgenstern, O., Nakamura, T., Olivie, D., Pawson, S., Pitari, G., Plummer, D. A., Pyle, J. A., Scinocca, J. F., Shepherd, T. G., Shibata, K., Smale, D., Teyssedre, H., Tian, W., and Yamashita, Y.: Using transport diagnostics to understand chemistry climate model ozone simulations, *J Geophys Res-Atmos*, 116, Artn D17302, 10.1029/2010jd015360, 2011.

- Tang, Q., and Prather, M. J.: Correlating tropospheric column ozone with tropopause folds: the Aura-OMI satellite data, *Atmos Chem Phys*, 10, 9681-9688, 10.5194/acp-10-9681-2010, 2010.
- Tang, Q., Hess, P. G., Brown-Steiner, B., and Kinnison, D. E.: Tropospheric ozone decrease due to the Mount Pinatubo eruption: Reduced stratospheric influx, *Geophys Res Lett*, 40, 5553-5558, 10.1002/2013GL056563, 2013.
- Tang, Q., Prather, M. J., Hsu, J. O., Ruiz, D. J., Cameron, P. J. S., Xie, S. C., and Golaz, J. C.: Evaluation of the interactive stratospheric ozone (O3v2) module in the E3SM version 1 Earth system model, *Geosci Model Dev*, 14, 1219-1236, 10.5194/gmd-14-1219-2021, 2021.
- Thompson, R. L., Patra, P. K., Ishijima, K., Saikawa, E., Corazza, M., Karstens, U., Wilson, C., Bergamaschi, P., Dlugokencky, E., Sweeney, C., Prinn, R. G., Weiss, R. F., O'Doherty, S., Fraser, P. J., Steele, L. P., Krummel, P. B., Saunio, M., Chipperfield, M., and Bousquet, P.: TransCom N2O model inter-comparison - Part 1: Assessing the influence of transport and surface fluxes on tropospheric N2O variability, *Atmos Chem Phys*, 14, 4349-4368, DOI 10.5194/acp-14-4349-2014, 2014.
- Tian, H. Q., Xu, R. T., Canadell, J. G., Thompson, R. L., Winiwarter, W., Suntharalingam, P., Davidson, E. A., Ciais, P., Jackson, R. B., Janssens-Maenhout, G., Prather, M. J., Regnier, P., Pan, N. Q., Pan, S. F., Peters, G. P., Shi, H., Tubiello, F. N., Zaehle, S., Zhou, F., Arneth, A., Battaglia, G., Berthet, S., Bopp, L., Bouwman, A. F., Buitenhuis, E. T., Chang, J. F., Chipperfield, M. P., Dangal, S. R. S., Dlugokencky, E., Elkins, J. W., Eyre, B. D., Fu, B. J., Hall, B., Ito, A., Joos, F., Krummel, P. B., Landolfi, A., Laruelle, G. G., Lauerwald, R., Li, W., Lienert, S., Maavara, T., MacLeod, M., Millet, D. B., Olin, S., Patra, P. K., Prinn, R. G., Raymond, P. A., Ruiz, D. J., van der Werf, G. R., Vuichard, N., Wang, J. J., Weiss, R. F., Wells, K. C., Wilson, C., Yang, J., and Yao, Y. Z.: A comprehensive quantification of global nitrous oxide sources and sinks, *Nature*, 586, 248-252, 10.1038/s41586-020-2780-0, 2020.
- Tokarska, K. B., Stolpe, M. B., Sippel, S., Fischer, E. M., Smith, C. J., Lehner, F., and Knutti, R.: Past warming trend constrains future warming in CMIP6 models, *Sci Adv*, 6, ARTN eaaz9549, 10.1126/sciadv.aaz9549, 2020.
- Tung, K. K., and Yang, H.: Global QBO in Circulation and Ozone 1. Reexamination of Observational Evidence, *J Atmos Sci*, 51, 2699-2707, Doi 10.1175/1520-0469(1994)051<2699:Gqicao>2.0.Co;2, 1994b.
- Tung, K. K., and Yang, H.: Global QBO in Circulation and Ozone 2. A Simple Mechanistic Model, *J Atmos Sci*, 51, 2708-2721, 10.1175/1520-0469(1994)051<2708:Gqicao>2.0.Co;2, 1994a.
- Williams, R. S., Hegglin, M. I., Kerridge, B. J., Jockel, P., Latter, B. G., and Plummer, D. A.: Characterising the seasonal and geographical variability in tropospheric ozone, stratospheric influence and recent changes, *Atmos Chem Phys*, 19, 3589-3620, 10.5194/acp-19-3589-2019, 2019.
- WMO: Scientific Assessment of Ozone Depletion: 2018, Global Ozone Research and Monitoring Project—Report No. 58, World Meteorological Organization, Geneva, Switzerland, 588 pp., 2018.
- Yang, H., Chen, G., Tang, Q., and Hess, P.: Quantifying isentropic stratosphere-troposphere exchange of ozone, *J Geophys Res-Atmos*, 121, 3372-3387, 10.1002/2015JD024180, 2016.
- Young, P. J., Archibald, A. T., Bowman, K. W., Lamarque, J. F., Naik, V., Stevenson, D. S., Tilmes, S., Voulgarakis, A., Wild, O., Bergmann, D., Cameron-Smith, P., Cionni, I., Collins,

W. J., Dalsoren, S. B., Doherty, R. M., Eyring, V., Faluvegi, G., Horowitz, L. W., Josse, B.,
 Lee, Y. H., MacKenzie, I. A., Nagashima, T., Plummer, D. A., Righi, M., Rumbold, S. T.,
 Skeie, R. B., Shindell, D. T., Strobe, S. A., Sudo, K., Szopa, S., and Zeng, G.: Pre-industrial
 to end 21st century projections of tropospheric ozone from the Atmospheric Chemistry and
 Climate Model Intercomparison Project (ACCMIP), *Atmos Chem Phys*, 13, 2063-2090,
 DOI 10.5194/acp-13-2063-2013, 2013.
 Young, P. J., Naik, V., Fiore, A. M., Gaudel, A., Guo, J., Lin, M. Y., Neu, J. L., Parrish, D. D.,
 Rieder, H. E., Schnell, J. L., Tilmes, S., Wild, O., Zhang, L., Ziemke, J., Brandt, J., Delcloo,
 A., Doherty, R. M., Geels, C., Hegglin, M. I., Hu, L., Im, U., Kumar, R., Luhar, A., Murray,
 L., Plummer, D., Rodriguez, J., Saiz-Lopez, A., Schultz, M. G., Woodhouse, M. T., and
 Zeng, G.: Tropospheric Ozone Assessment Report: Assessment of global-scale model
 performance for global and regional ozone distributions, variability, and trends, *Elementa-
 Science of the Anthropocene*, 6, 2018.
 Zeng, G., Morgenstern, O., Braesicke, P., and Pyle, J. A.: Impact of stratospheric ozone recovery
 on tropospheric ozone and its budget, *Geophys. Res. Lett.*, 37, L09805,
 10.1029/2010gl042812, 2010.
 Ziemke, J. R., Oman, L. D., Strobe, S. A., Douglass, A. R., Olsen, M. A., McPeters, R. D.,
 Bhartia, P. K., Froidevaux, L., Labow, G. J., Witte, J. C., Thompson, A. M., Haffner, D. P.,
 Kramarova, N. A., Frith, S. M., Huang, L. K., Jaross, G. R., Seftor, C. J., Deland, M. T., and
 Taylor, S. L.: Trends in global tropospheric ozone inferred from a composite record of
 TOMS/OMI/MLS/OMPS satellite measurements and the MERRA-2 GMI simulation,
Atmos Chem Phys, 19, 3257-3269, 10.5194/acp-19-3257-2019, 2019.